



Properties and Corrosion Resistance of AISI H13 Hot-Work Tool Steel with Borided B₄C Powders

Ali Günen¹ · İsmail Hakki Karahan² · Mustafa Serdar Karakaş³ · Bülent Kurt⁴ · Yusuf Kanca⁵ · Vedat Veli Çay⁶ · Murat Yıldız⁷

Received: 12 March 2019 / Accepted: 5 August 2019 / Published online: 9 August 2019
© The Korean Institute of Metals and Materials 2019

Abstract

In this study, the surface of AISI H13 steel was borided with powder blends of B₄C and NaBF₄ using the powder-pack method at 800, 900 and 1000 °C for 2, 4 and 6 h. The structural and mechanical characteristics of the boride layers formed on the surface were characterized using scanning electron microscopy, energy dispersive spectroscopy, X-ray diffractometry, 2D surface profilometry, microhardness and electrochemical corrosion (3.5 wt% NaCl) tests. The boride layer exhibited a single phase structure (Fe₂B) in samples coated at 800 °C and a dual-phase structure (FeB + Fe₂B) at higher boriding temperatures (900 and 1000 °C). The boride layers were compact and crack-free in all boriding conditions. Depending on boriding parameters, the thickness, hardness and average surface roughness (R_a) of the coatings were found to range between 5.81 and 102.46 μm, 1635–1915 HV and 0.315–0.650 μm, respectively. The borided AISI H13 steel displayed up to 33.5 times and 2.4 times higher corrosion resistance than untreated AISI H13 steel and martensitic AISI 431 steel, respectively. This suggests potential use of borided AISI H13 steel in the steam turbines and marine applications as an alternative to the more costly martensitic and duplex stainless steel grades. The corrosion resistance depended on the phase structure (single- or dual-layer), density, thickness and surface roughness of the boride coatings.

Keywords Steel · Boriding · Corrosion · NaCl

1 Introduction

The tailorable mechanical properties of steels have enabled them to become the most widely used material group in the industry [1, 2]. However, issues such as corrosion and wear under extreme service conditions often restrict their service life [3, 4] and cause vital economic losses. Since corrosion and wear events generally start at the surface of a material and proceed towards the interior, techniques aimed at enhancing the wear and corrosion resistance of the surface instead of the bulk are usually more cost effective [3, 5]. Surface modification introduces a practical and economical approach while simultaneously offering greater lifespan [6]. Research on surface modification techniques has been increasing over the last two decades [5].

Boriding is considered as one of the most effective surface modification techniques to improve the mechanical properties and corrosion resistance of metals and their alloys. It is a thermochemical surface treatment in which boron diffuses into the substrate material, forming hard, highly adherent boride layers on the substrate. The

✉ Ali Günen
aligunen2013@gmail.com; ali.gunen@iste.edu.tr

¹ Department of Metallurgy and Materials Engineering, Faculty of Engineering and Natural Sciences, Iskenderun Technical University, 31200 Hatay, Turkey

² Department of Physics, Faculty of Science and Arts, Mustafa Kemal University, 3100 Hatay, Turkey

³ Department of Metallurgical and Materials Engineering, Faculty of Engineering and Natural Sciences, Konya Technical University, 42130 Konya, Turkey

⁴ Department of Materials Engineering, Faculty of Engineering and Architecture, Nevşehir Hacı Bektaş Veli University, 50000 Nevşehir, Turkey

⁵ Department of Mechanical Engineering, Faculty of Engineering, Hitit University, 19030 Çorum, Turkey

⁶ School of Civil Aviation, Dicle University, 21280 Diyarbakir, Turkey

⁷ Department of Mechanical Engineering, Faculty of Engineering and Natural Sciences, Iskenderun Technical University, 31200 Hatay, Turkey

technique introduces the growth of a hard surface layer consisting of boron compounds [5]. Iron borides (such as FeB and Fe₂B) formed on steel possess higher hardness and better tribological performance than conventional surface treatments (i.e., carburizing, nitriding and carbonitriding) [7]. The borides formed also influence the corrosion potential of steels [6, 8–11].

The phase structure and morphology of boride layers grown on steels depend directly on the chemical composition of substrate and boriding powders used, as well as the treatment environment, temperature and time [5]. Boriding of iron alloys is generally performed at the temperatures of 850–1000 °C for 1–10 h [12]. The boron potential in the boriding medium is what mainly determines the type of boron/boride layer, which could be obtained in the form of Fe₂B (tetragonal 8 wt% B) and/or FeB (orthorhombic, 16 wt% B) [13]. FeB has higher hardness and stiffness but lower toughness than Fe₂B [14]. FeB and Fe₂B have different thermal expansion coefficients ($23 \times 10^{-6} \text{ }^\circ\text{C}^{-1}$ and $7.85 \times 10^{-6} \text{ }^\circ\text{C}^{-1}$, respectively); therefore, transverse and/or longitudinal cracks can form at the FeB/Fe₂B interfaces. The saw-tooth morphology at the interfaces of Fe₂B/substrate enables stronger adherence [13, 14]. The corrosion resistance of borided steel is influenced by many characteristics of coating, such as phase structure (single- or dual-layer), porosity and microcracking [8–11]. The penetration of corrosive media from a porous or cracked boride layer to base material could lead a failure at the interfaces of coating/substrate, leading to the delamination of the coating layer from the substrate [15].

Boride coatings have a prominent place especially in tribological industrial applications [5, 6]. Although boriding treatments were applied primarily to ferrous alloys (carbon steels, tool steels, stainless steels, etc.) they are recently being applied to many other alloys including non-ferrous metals, cermets and superalloys [16]. However, considering the literature, it is noteworthy that studies on the mechanical behavior of borided materials are more widespread [6, 7, 12, 14, 16–18] than those on corrosion behavior, and most of the corrosion studies are focused on the corrosion of borided steels such as low carbon, AISI M2, AISI 1018, AISI 304, case-hardening steels and cold work tool steels, etc. in HCl acid solutions [19–22]. Despite the fact that many borided steels have use in NaCl environments, their corrosion behavior in NaCl environment is relatively less studied and the majority of these

studies are limited to low carbon steels and AISI 304 stainless steel [15, 23–25].

Hot-work tool steels are largely employed in industrial processes that take place in aggressive environments. AISI H13 steel, for example, is commonly used in the fabrication of dies, moulds, cores, die holder blocks, and screws for poly(vinyl chloride) (PVC) extrusion mandrels, injection moulds, gears and rolls [7]. One drawback associated with the high temperature processing of PVC-containing materials are the non-negligible concentrations of free chloride species originating from the cleavage of C–Cl bonds, which can strongly accelerate corrosion and wear [26]. However, the corrosion behavior of borided AISI H13 steel in NaCl solutions has not been extensively studied. Therefore, the purpose of the current work was to investigate the electrochemical corrosion behavior of borided AISI H13 steel (borided at various temperatures and durations) in 3.5 wt% NaCl solution.

2 Experimental Methods and Materials

AISI H13 hot work tool steel was used as the substrate material for the boriding process. As stated in the technical data sheet, the AISI H13 samples were annealed at 850 °C for 2 h, which had a hardness of 510 ± 10 HV. AISI 431 martensitic stainless steel, which is indispensable in steam turbines and marine applications, was chosen for comparison in the corrosion tests [27]. The AISI 431 specimens were subjected to a sequence of heat treatments, as specified in the technical data sheet. They were first austenitized at 1050 °C for 2 h followed by quenching, and then tempered at 650 °C for 1 h followed by cooling in air, which had a hardness of 295 ± 15 HV. Table 1 shows the chemical compositions of both alloys, obtained from a Thermo Jarrell Ash/Baird DV-6S 3063A spectral analyser.

Due to the relatively high Si content in the H13 steel, a boriding mixture free of Si-containing compounds was used [28]. The boriding agent consisted of 95 wt% B₄C as the boriding source and 5% NaBF₄ as the activator. Particle sizes of B₄C powder were determined using a Malvern Mastersizer 2000 (Malvern, Worcestershire, UK), equipped with a Hydro2000S sample dispersion unit. An SEM image of the B₄C powder is provided in Fig. 1.

Prior to boriding, the specimens were cut to dimensions of 30 × 30 × 5 mm. After grinding with 1200 mesh SiC

Table 1 Chemical composition (wt%) of the AISI H13 hot work tool steel and AISI 431 martensitic stainless steel used in experimental studies

Sample	Cr	Ni	Mo	V	Si	C	Mn	Fe
AISI H13	5.25	–	1.65	1.10	1.0	0.40	0.35	Balance
AISI 431	17.5	2.5	–	–	1.0	0.15	1.0	Balance

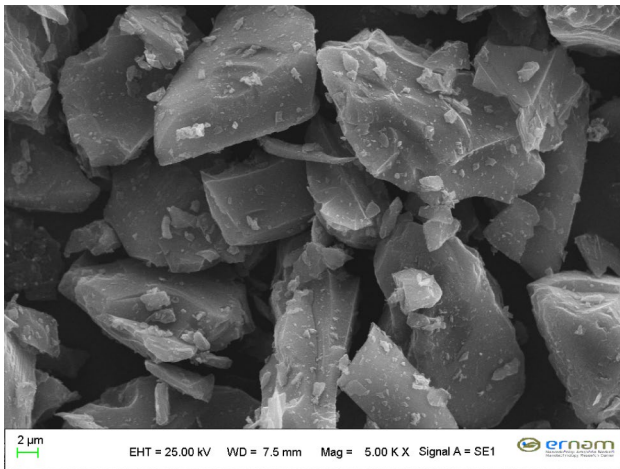


Fig. 1 SEM view of the used B_4C boriding agent

abrasive paper the specimens were washed with distilled water, ultrasonically degreased in acetone for 15 min and rinsed in alcohol. The samples were then packed with the boriding powder in a stainless steel container and the top of the container was covered with very fine Al_2O_3 powders to prevent oxidation. The boriding process was carried out at temperatures of 800 °C, 900 °C and 1000 °C for 2, 4 and 6 h, and the borided samples were then removed from furnace and cooled to room temperature in air. A fresh boriding agent used for each boriding condition.

For metallographic examinations, borided samples of appropriate size were cut and cross-sectional surfaces were cold-mounted. The specimens were then ground using 320–1500 grit SiC abrasive paper and polished with 3 μm alumina paste followed by 1 μm diamond paste to achieve a good mirror finish. After polishing, the samples were etched in a 3.5 wt% Nital solution to reveal microstructural details.

Metallographic studies were conducted on polished and etched cross-sections of the specimens and on corroded surfaces using a TESCAN MAIA3 XMU high resolution Field Emission Scanning Electron Microscope (FESEM) equipped with Energy Dispersive Spectroscopy (EDS) capability, operating at an accelerating voltage of 25 kV. Microhardness measurements were recorded using a Future-Tech FM-700 hardness tester with a Vickers pyramid indenter along the cross-section using 100 g load and 15-s dwell time. The average of 5 measurements was recorded for each experimental condition. The thicknesses of boride layers were measured by FESEM and the presence of the boride phases formed on the surface was confirmed by X-ray diffraction (XRD) analyses using a computer-controlled RIGAKU Smart Lab™ diffractometer, with $CuK\alpha$ radiation ($\lambda = 0.154$ nm), 2θ ranging from 10° to 90°, step size of $\Delta 2\theta = 0.006^\circ$, and integration time of 280 s. A Hommel Tester T8000 profilometer was

used to evaluate the surface roughness of the samples with at the speed of 2 mm/s across a sampling length of 5.0 mm.

The corrosion performances of untreated AISI 431, untreated AISI H13, and AISI H13 borided under different boriding parameters were analysed in a 3.5% NaCl solution using a CH 608E analyzer. Open-circuit potential (OCP) and potentiodynamic polarization curves of the samples were obtained at room temperature in a three-electrode corrosion cell. The corrosion cell consisted of a reference electrode, a counter electrode, and the test sample mounted to a Teflon holder in a corrosion solution as the working electrode. The OCP was measured over 1 h, and was plotted as a function of time after stabilisation. Potentiodynamic corrosion tests were performed below or above -250 mV of the OCP value at a potential scanning rate of 0.1 mV as stated in a previous study [8]. Each test was repeated three times, and the corrosion test results reported represent averages from three measurements. The surface area of the test coupons exposed to the electrolyte was 0.785 cm². After corrosion testing, the surface of each sample was using FESEM following mechanical cleaning.

3 Results and Discussion

3.1 Metallographic Analysis

Cross-sectional SEM images of the microstructures of the specimens, borided under 800, 900 and 1000 °C temperatures for 2, 4 and 6 h with B_4C powder, are shown in Fig. 2. The boride layer formed on the substrate surfaces after the boriding process conducted at 800 °C displays inconsistencies in thickness (Fig. 2a–c). This is attributed to the annealing temperature of AISI H13 steel, which is between 830 and 850 °C [1]. For the specimens borided at 1000 °C and 1100 °C, the boride layer formed on the substrate surface is more uniform and continuous (Fig. 2d–i). Moreover, increase in boriding temperature and time resulted in an increase in the thickness and density of the coatings [6, 7, 29].

The samples with different layer morphologies were subjected to both XRD and EDS analyzes in order to determine their phase contents. XRD analyzes show that the predominant phase is single-phase Fe_2B in samples borided at 800 °C, and a double-phase layer of $FeB + Fe_2B$ in the samples borided 900 and 1000 °C. In addition, a low amount of CrB phase was formed in all experimental conditions (Fig. 3). A low proportion of MoB phase was detected in borided samples at 800 °C. Increasing the boriding time from 2 h to 4 h at 800 degrees allowed the Fe_2B phase to appear, leading to a reduction in the orientation of the CrB phase (Fig. 3d–f). For the same boriding time (4 h), the temperature increased by 100 degrees, and caused the Fe_2B

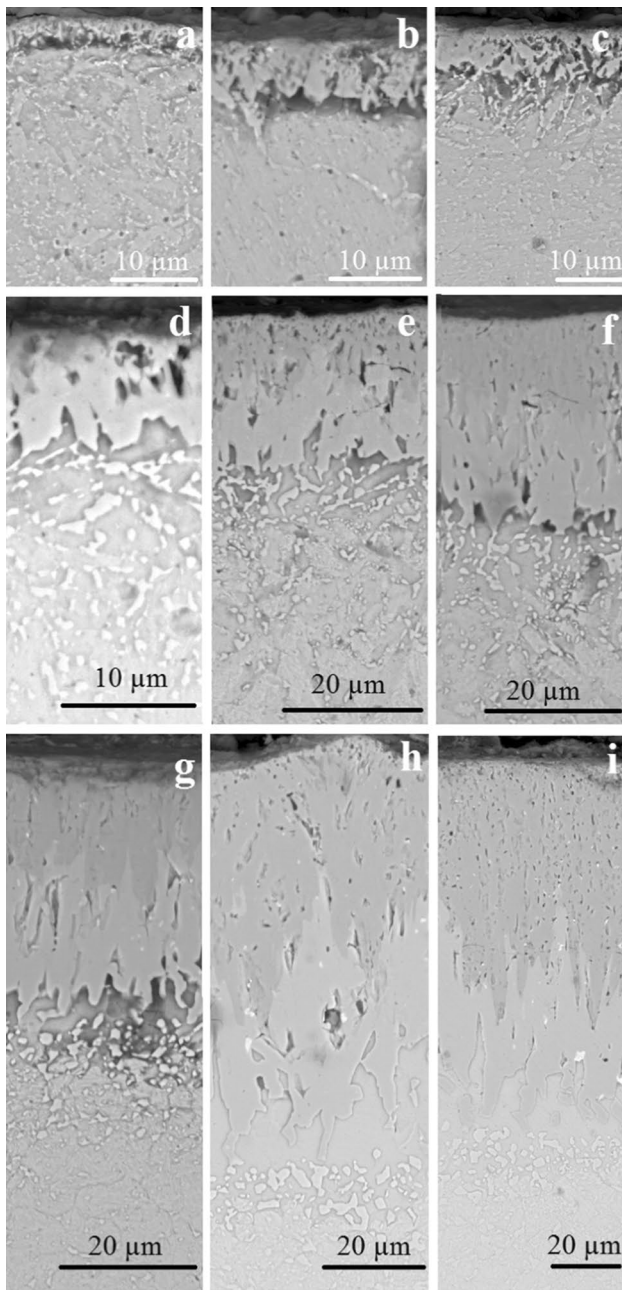


Fig. 2 Cross-section SEM images of borided AISI H13 steel after **a** 800 °C for 2 h, **b** 800 °C for 4 h, **c** 800 °C for 6 h, **d** 900 °C for 2 h, **e** 900 °C for 4 h, **f** 900 °C for 6 h, **g** 1000 °C for 2 h, **h** 1000 °C for 4 h and **i** 1000 °C for 6 h

phase to decrease in orientation and the FeB phase to occur. It is seen that the intensity of the other phases (Fe_2B , CrB) decreases and even some of them disappear (MoB) due to the increase in FeB layer thickness in borided samples at 900 and 1000 °C. This shows that XRD rays penetrate to a certain depth from the surface. As a result, the SEM and EDS images show that the phase (Fe_2B), which is clearly visible at the base of the coating, is detected to a lesser extent. Even

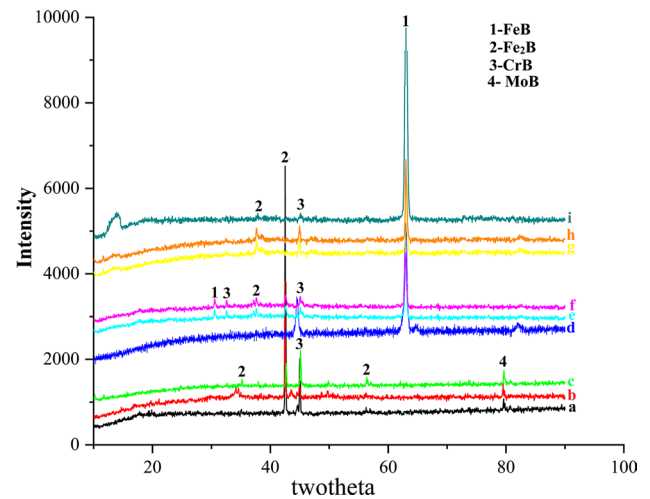


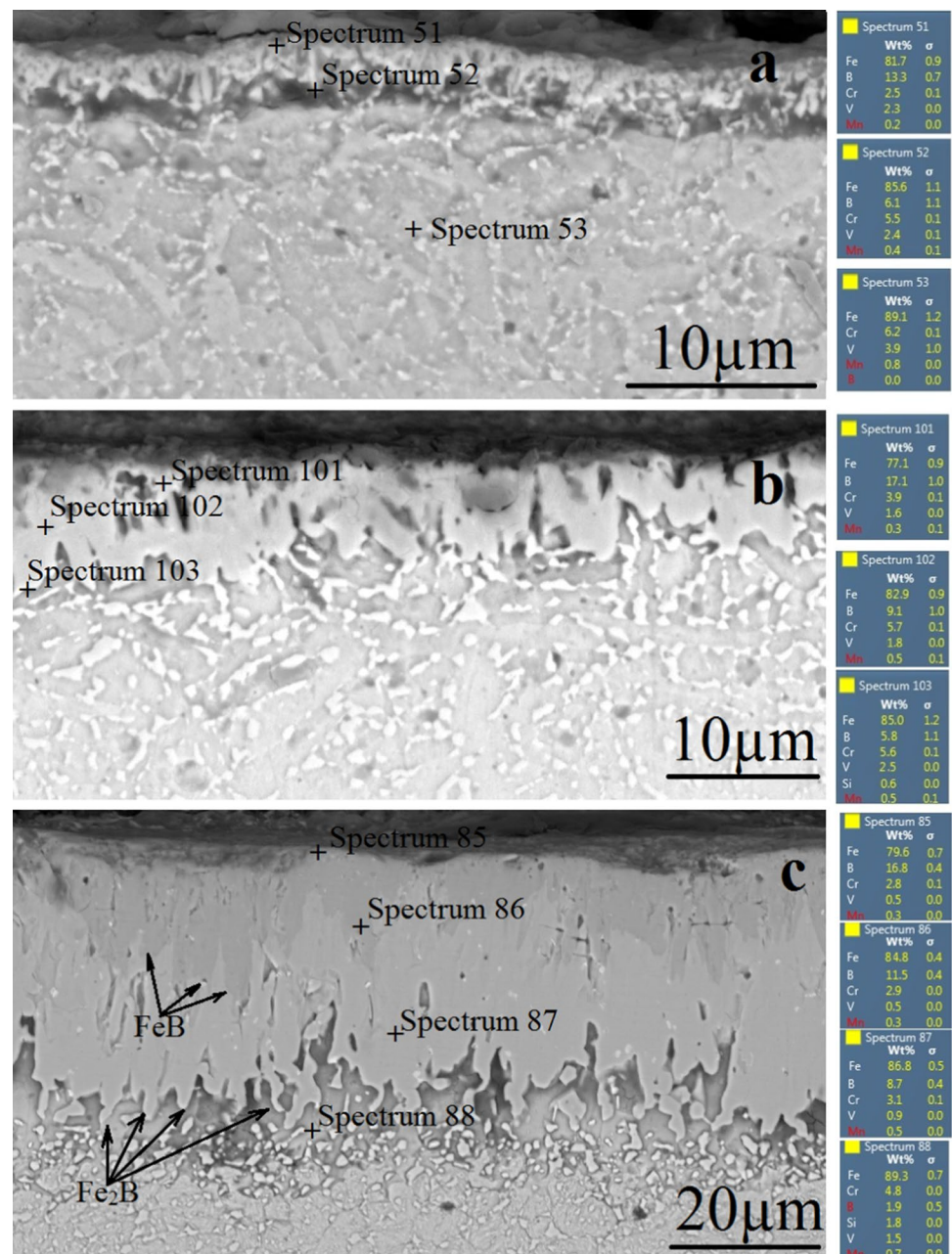
Fig. 3 XRD analyses of borided samples at **a** 800 °C for 2 h, **b** 800 °C for 4 h, **c** 800 °C for 6 h, **d** 900 °C for 2 h, **e** 900 °C for 4 h, **f** 900 °C for 6 h, **g** 1000 °C for 2 h, **h** 1000 °C for 4 h and **i** 1000 °C for 6 h

in the literature, it has been shown that Fe_2B phase may not be detected in an XRD pattern due to the thick FeB layer [30].

Formation of borides on the surfaces of the samples was verified by EDS analysis. A FeB layer appeared as a dark-etched zone at the outermost sections, whereas the Fe_2B layer appeared as a bright-etched zone just below FeB layer (Figs. 2, 4c) [12, 30]. The dark regions (FeB) had more than 16 wt% B (Spectrum 85, Spectrum 101), and ratio of boron decreased to 5.8–13 wt% content (Spectrum 85, Spectrum 51, Spectrum 52, Spectrum 86, Spectrum 87, Spectrum 102) in the lighter regions (Fe_2B) (Fig. 4). These ratios are consistent with FeB (16.23 wt% B) and Fe_2B (8.93 wt% B), which is in line with the literature. EDS results further indicate increasing concentrations of Fe, Cr, V, Si with increasing depth [7], meaning that during the boriding process, these elements are swept towards the interior as Fe reacts with B, which also explains the absence of other borides such as MnB and VB.

The thickness, hardness and surface roughness of the boride layers as a function of boriding temperature and time are listed in Table 2. The thickness of the boride layers in the specimens ranged from 5.81 to 102.46 μm and the hardness values ranged from 1615 to 1935 $\text{HV}_{0.1}$. The increase in boriding time and temperature resulted in an increase in boride layer thickness and hardness values as stated in the previous study [6, 7, 12, 30, 31]. The surface roughness test results show a decrease in surface roughness with increasing boriding temperature. The observed decrease is not in line with previous studies [32, 33] and can be attributed to the discontinuous nature of the boride layer at lower (800 °C and 900 °C) boriding

Fig. 4 EDS analyses of the borided samples for 2 h **a** 800 °C, **b** 900 °C and **c** 1000 °C



temperatures. A continuous, pore-free boride layer could only be obtained at 1000 °C, and it is likely that the surface roughness would increase at boriding temperatures beyond 1000 °C. Another difference from the previous study is that a crack-free boride layer is obtained, albeit with lower hardness due to the absence of harder borides such as VB, and MnB [7, 34]. The surface roughness should be kept to a minimum since very small crevices on the surface can serve as initiation sites for corrosion in many cases [8].

3.2 Corrosion Test Results

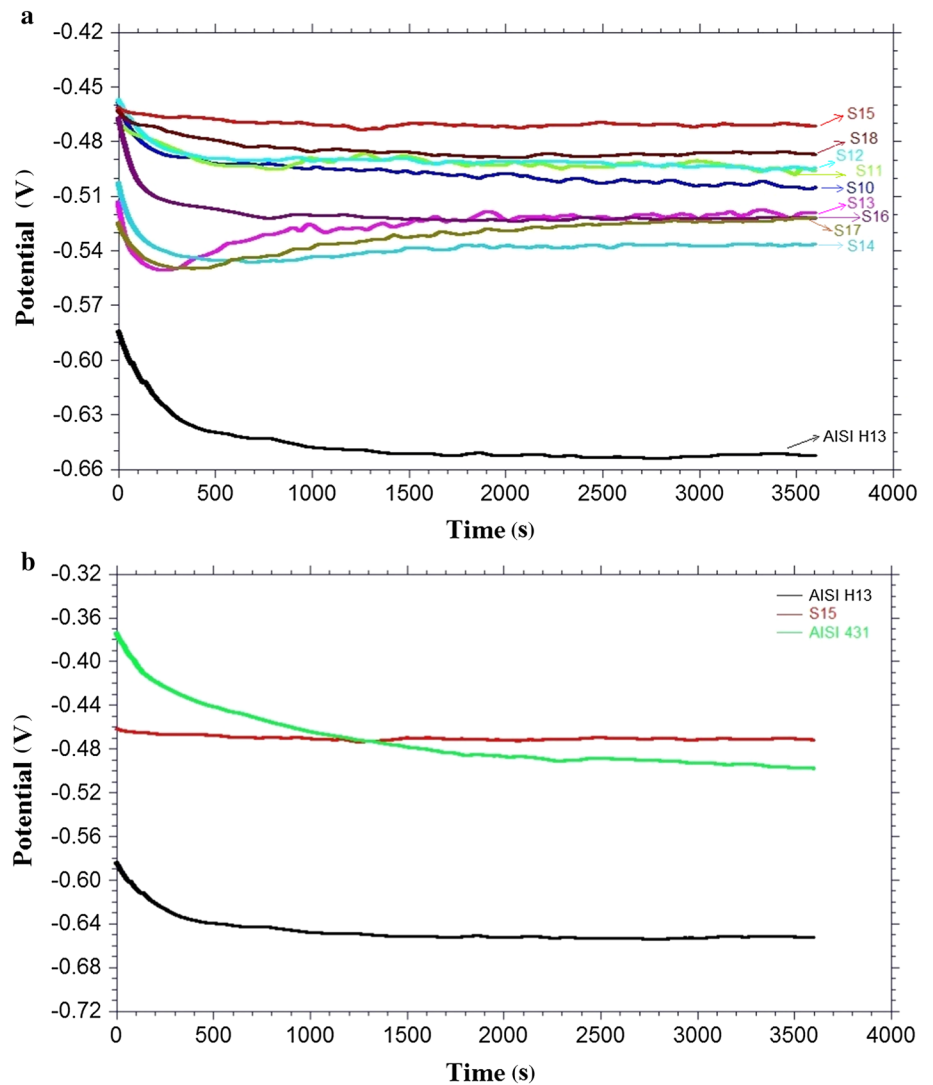
3.2.1 Open Circuit Potential Curves

Open circuit potential potentiodynamic polarization measurements were made in 3.5% NaCl to compare the corrosion performances of the borided AISI H13 steels with untreated AISI 431. A less negative potential in an open circuit potential test is often considered a measure of corrosion resistance; the more negative the potential, the lower the corrosion resistance of the surface [8]. When the open-circuit potentials of the samples S10, S11, and S12 (samples borided

Table 2 The thickness, surface hardness and roughness of the coatings at different boriding temperatures and durations

Sample	Treatment temperature (°C)	Treatment duration (h)	Coating thickness (μm)	Surface hardness ($\text{HV}_{0.05}$)	Surface roughness ($R_a, \mu\text{m}$)
S10	800	2	5.81 ± 0.8	1635 ± 125	0.65
S11		4	7.62 ± 0.7	1653 ± 92	0.46
S12		6	9.64 ± 0.7	1665 ± 70	0.52
S13	900	2	9.70 ± 1.1	1725 ± 105	0.340
S14		4	25.44 ± 1.8	1784 ± 78	0.368
S15		6	32.17 ± 3.1	1791 ± 25	0.315
S16	1000	2	39.84 ± 2.7	1805 ± 60	0.345
S17		4	70.08 ± 3.6	1850 ± 23	0.352
S18		6	102.46 ± 2.1	1915 ± 21	0.327
S19	Untreated AISI H13		510 ± 10		0.25
S20	Untreated AISI 431		295 ± 15		0.25

Fig. 5 Open circuit potential versus time plots comparing **a** untreated and borided AISI H13 steels; **b** untreated AISI H13, untreated AISI 431 and sample S15



at 800 °C for 2–6 h) are compared, it is seen that the open circuit potentials of the borided samples are positioned at more stable values compared to untreated AISI H13 at around -0.49 V. Moreover, the samples display increasing potentials with increasing boriding time (Fig. 5).

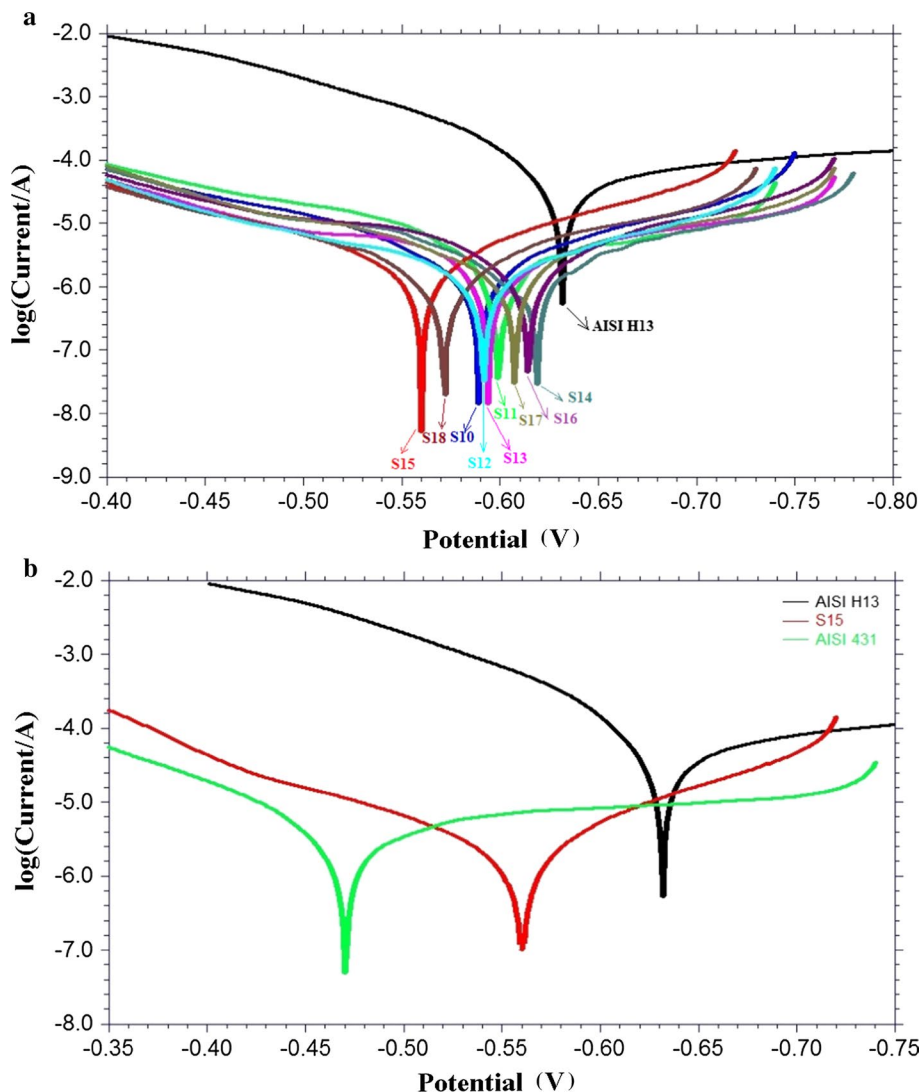
The open circuit potential plots for samples S13, S14 and S15 (samples borided at 900 °C for 2–6 h) also exhibit corrosion resistances superior to untreated AISI H13 steel. Sample S13, which does not fit the general trend, displays an initial decrease in open circuit potential from -0.517 to -0.550 V in the first 250 s, followed by a steady increase towards -0.520 V. This indicates dynamic changes in the system. The open circuit potential initially decreases as a result of corrosion beginning at the surface. After about 250 s the open circuit potential increases and the corrosion rate begins to decrease. As time progresses the open circuit potential reaches a stable value of -0.520 V, indicating the formation of a passive film on the surface. Sample 14, borided at 900 °C for 4 h, displays the lowest corrosion resistance among the

borided samples, probably because of its high surface roughness, Table 2. On the other hand, sample S15 (900 °C for 6 h) displays the most stable open circuit potential value among all the borided samples from beginning to end, and shows values comparable to AISI 431 steel in Fig. 5b. Surface roughness appears to be very beneficial for the effectiveness of the boride layer, the initial surface roughness of sample S15 is the lowest among all borided samples. Samples S16, S17 and S18 (samples borided at 1000 °C for 2–6 h) are also more stable compared to the untreated AISI H13 steel, but the corrosion resistance does not increase with boriding time. Sample S17, borided at 1000 °C for 4 h displays the lowest corrosion resistance among the three samples, and behavior similar to sample S13, due to high initial surface roughness [8].

3.2.2 Potentiodynamic Polarization Curves

Polarization plots for the untreated and borided AISI H13 steels are presented in Fig. 6. It is seen from the plots that

Fig. 6 Polarization curves for **a** untreated and borided AISI H13 steels; **b** untreated AISI H13, untreated AISI 431 and sample S15



while the untreated AISI H13 steel displays a stable corrosion potential of -0.632 V, the corrosion potentials of samples S10, S11, and S12 display potentials of -0.589 , -0.599 and -0.592 V, respectively. This indicates that the boride layer is, to some degree, capable of protecting the steel from the corrosive medium. Kariofillis et al. [11] have observed similar results for borided AISI H13 steels tested in 5 vol%, 5 vol% H_2SO_4 and 30 vol% H_3PO_4 solutions. There are also other studies that show that boriding improves the corrosion resistance steels in NaCl [15, 23–25].

When samples S10, S11 and S12 are compared, S10 exhibits better corrosion resistance compared to both S11 (where a single-phase Fe_2B layer is present on the surface) and S12 (where a double-phase boride layer is present). It has been stated in the literature that a single-phase layer consisting solely of Fe_2B could provide better corrosion resistance than a double-phase $FeB + Fe_2B$ layer due to microcracking that may occur in the double-phase coating as a result of the large difference in the coefficient of thermal expansion (CTE) between FeB ($23 \times 10^{-6} \text{ }^\circ\text{C}^{-1}$) and Fe_2B ($7.85 \times 10^{-6} \text{ }^\circ\text{C}^{-1}$), which reduces the overall effectiveness of the boride coating [13, 24]. It should be noted, however, that SEM images of the borided surfaces in Fig. 1 reveal that the coatings are free of CTE microcracks. On the other hand, both open circuit potential and polarization curves display strong dependence on initial surface roughness. Samples with lowest surface roughness (e.g. sample S15) show higher corrosion resistance compared to samples with low surface roughness (e.g. sample S14). While no porosity or microcracking may be present on the surface, small pits or undulations on the surface may act as starting points for localized corrosion [8, 15].

The polarization curves also show an increase in corrosion with boriding, in agreement with the open circuit potential curves, that the corrosion potentials (E_{corr}) are shifted towards more positive values and the corrosion current densities are decreased with the boriding treatment. It can be also deduced from both Figs. 5 and 6 that the corrosion resistance of borided AISI H13 steel approaches the corrosion resistance of AISI 431.

Table 3 shows that the measured corrosion current density (i_{corr}) values for samples subjected to corrosion testing in 3.5% NaCl range between 2.589×10^{-6} A and 9.030×10^{-5} A. The corrosion current densities of all borided samples are lower than that of untreated AISI H13 steel and AISI 431 steel. The corrosion potential (E_{corr}) values range between -0.619 and -0.560 V. The values measured for AISI H13 and AISI 431 steel are -0.631 and -0.470 V, respectively. Both i_{corr} and E_{corr} values indicate that the corrosion resistance of the H13 steel can be improved to reach the corrosion resistance of martensitic AISI 431 steel. Open circuit potential tests in Fig. 5b further indicate that while AISI 431 initially corrodes while forming

Table 3 Corrosion data for untreated and borided AISI H13 steels (obtained from Fig. 6) using the Tafel extrapolation method

Numune	E_{corr} (V)	I_{corr} (A) 10^{-6}	Corrosion rate (g/h) 10^{-6}
S10	-0.589	2.990	3.124
S11	-0.599	4.511	4.713
S12	-0.592	2.589	2.705
S13	-0.594	5.030	5.255
S14	-0.619	4.243	4.433
S15	-0.560	3.074	3.211
S16	-0.614	5.075	5.302
S17	-0.607	4.350	4.544
S18	-0.572	2.613	2.730
AISI H13	-0.632	90.295	90.711
AISI 431	-0.470	6.250	6.530

Corrosion data for untreated AISI 431 is also given for comparison

a protective passive layer, the borided AISI H13 remains at high potential throughout the test. In the initial 1300 s, the open circuit potential for AISI 431 is higher than the open circuit potential for S14, but beyond 1300 s the open circuit potential for S14 meets and exceeds the potential for AISI 431, indicating the potential of borided H13 steels in corrosive environments. It is well known [30] that AISI H13 steels are commonly used in hot forging processes, and that AISI H13 steels are susceptible to failures due to erosion and thermal cycling. Boriding may be a suitable surface modification treatment for protecting the surface of AISI H13 against erosion failures, provided that thermal cycling is kept at a minimum.

3.2.3 Examination of Corroded Surfaces and Microstructure

After corrosion testing, the corroded surfaces of the untreated AISI H13 and a few of the borided samples (S10, S13 and S16) were subjected to SEM and EDS analyses, the results of which are presented in Figs. 7, 8, 9 and 10.

When the SEM and EDS results for the borided samples are compared, one notable finding, other than the evidence of corrosion, is the presence of boron. This means that the boride layers persist on the surface of the borided samples. In addition, the corrosion products, the intact boride layers and the corroded AISI H13 matrix can be distinguished from one another. When the EDS spectra from the less-corroded regions of the borided samples are examined, the first three elements in highest concentration are ranked as O, Fe and B. However, when the spectra from preferentially corroded areas (Spectrum 206 in Fig. 7, Spectrum 213 and 215 in Fig. 8, and Spectrum 219 in Fig. 9) are compared, they reveal higher concentrations of B. Concentrations of Cr, V

Fig. 7 SEM image and EDS analysis of the sample S10 following the corrosion test

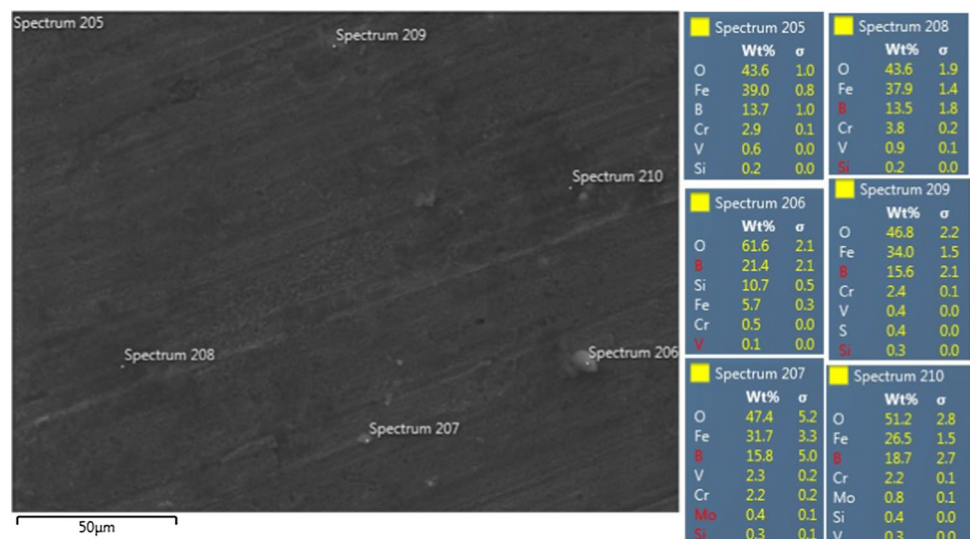
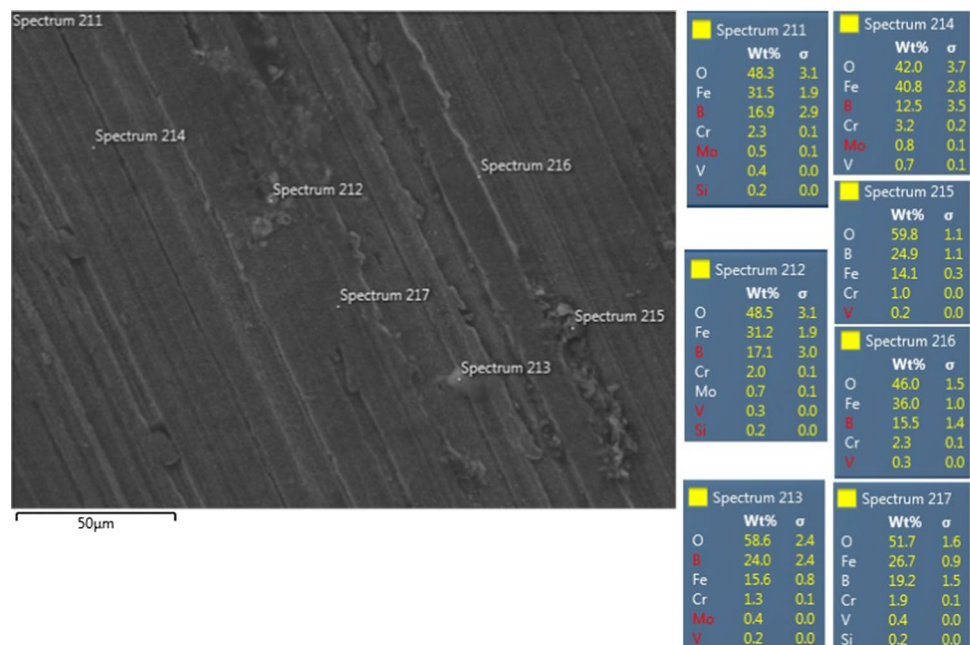


Fig. 8 SEM image and EDS analysis of the sample S13 following the corrosion test



Si and Mo were found to vary considerably between different regions; similar results have been reported by Bolelli et al. [35].

When the SEM images and EDS spectra of the untreated AISI H13 are taken into consideration, the first three elements in highest concentration at the surface are revealed as Fe, O and Cr. The existence of relatively high concentrations of B and O on the surfaces of the corroded surfaces of the borided AISI H13 steel indicates the possibility of B_2O_3 formation on the surface. The fact that borided AISI H13 steel displays better corrosion resistance compared to untreated AISI H13 and corrosion resistance comparable to AISI 431 indicates that B_2O_3 formation has a beneficial

effect on the corrosion resistance, an effect similar to that of Cr_2O_3 in stainless steels.

Further observations using XRD were carried out on the corroded surfaces to confirm our findings detected in EDS analysis about the formation of the oxide-containing (Fe_xO_y , B_xO_y and Cr_xO_y) compounds.

As can be clearly seen from Fig. 11, the XRD spectra showed the formation of Fe_2O_3 and Fe_3O_4 phases in all samples subjected to corrosion testing. Fe_2O_3 was the dominant phase in both uncoated and boronized AISI H13 (Fig. 11a, c). Whilst, Cr_2O_3 was dominant in untreated AISI 431 steel (Fig. 11b), which can be attributed to the high Cr-content of 431 stainless steel. In addition to iron oxide phases (Fe_2O_3 and Fe_3O_4), iron boride layers (FeB and Fe_2B) were

Fig. 9 SEM image and EDS analysis of the sample S16 following the corrosion test

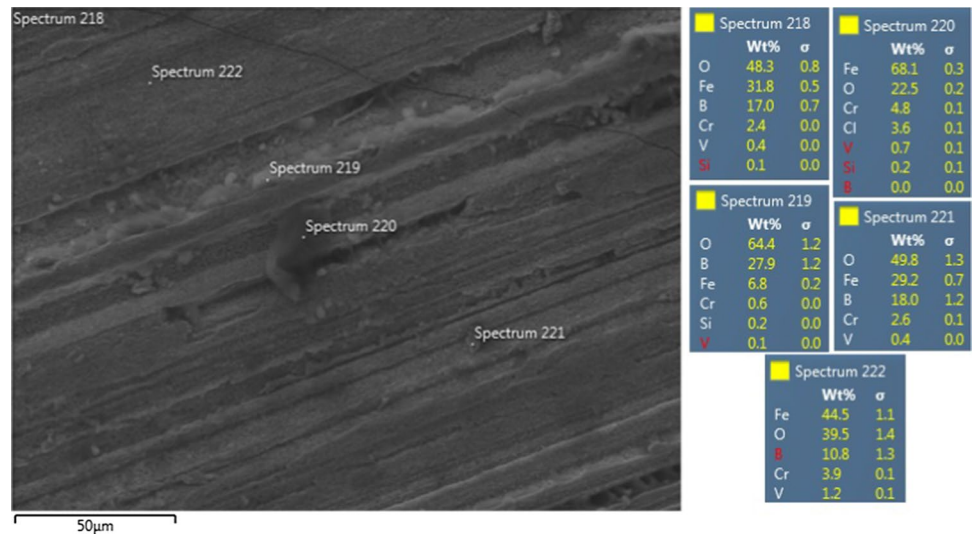
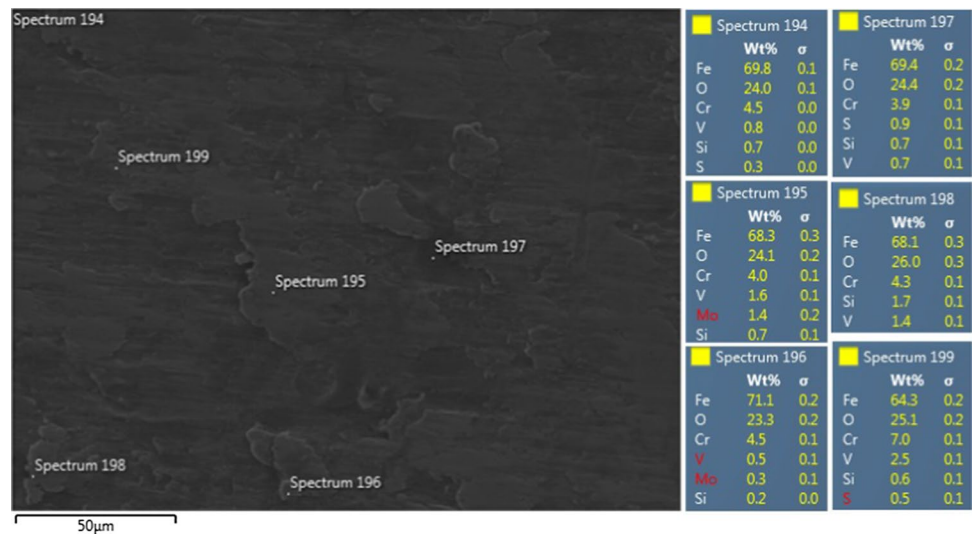


Fig. 10 SEM image and EDS analysis of the untreated AISI H13 sample following the corrosion test



determined on the surface of the boronized samples after corrosion testing (Fig. 11c). These boride phases were also detected by XRD analysis of the boronized sample before the corrosion test (Fig. 3). XRD results confirm the existence of the B_2O_3 barrier effect and iron boride layers (FeB and Fe_2B) on boronized AISI H13 surface after corrosion testing observed by EDS.

SEM imaging of corroded cross-sections were made to further understand the effects of the corrosion process (Fig. 12a, b).

When the Fig. 12 is examined, it is seen that the corrosion liquid has accumulated in the pits in the non-borided sample. It has been found that the corrosion event occurs homogeneously in the non-borided sample. In the sample S18 which has the highest coating layer, it is seen that the corrosive liquid affects approximately 20–25 μm of the boride layer

and the inner part of the boride layer is not affected by the corrosion solution.

In the S18 sample, it is seen that the progression of the corrosion liquid into the interior is not equal on all sides of the surface (shallow in some regions and deeper in some regions). This can be attributed to a number of reasons such as;

1. The difference between Ra (Table 2) and Rz values due to the process being controlled by diffusion as a result of increasing surface roughness values after boriding process
2. The phases formed in the coating layer (FeB , Fe_2B , CrB etc.) not being homogeneous everywhere and the corrosion resistance of the phases being different as a result.
3. The formation of capillary cracks during cooling due to the formation of different boride phases with differ-

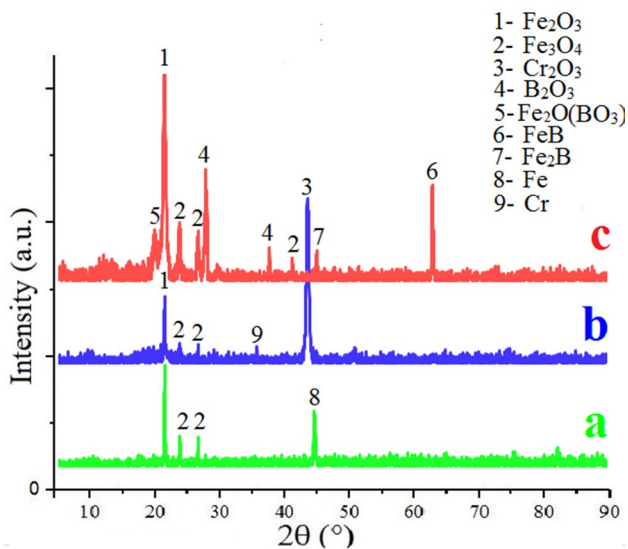


Fig. 11 The XRD patterns of the samples corrosion-tested in NaCl solution: **a** untreated AISI H13 (S19), **b** untreated AISI 431 (S20), and **c** boronized AISI H13 (S15)

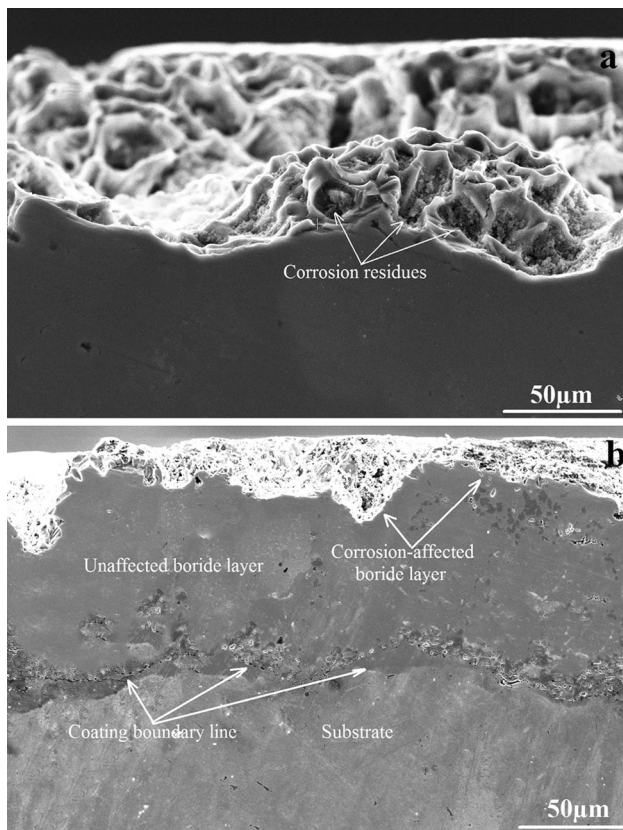


Fig. 12 Cross-section SEM images of **a** non-borided AISI H13 and **b** S18 after corrosion test

ent thermal expansions in the boriding layers, and the possibility that the corrosive liquid might have utilized those cracks to find paths.

4 Conclusions

In this study, AISI H13 type hot work steel was pack borided at temperatures of 800, 900 and 1000 °C for 2, 4, and 6 h using %95 B₄C + %5 NaBF₄ powders. The effects of boriding parameters on the mechanical properties and corrosion resistance of the boride layer were investigated. The conclusions obtained from the results are summarized as follows:

1. Boride layers were successfully grown on the surface of the AISI H13 steel. The boride layer displayed the typical sawtooth morphology, and was free of microcracks.
2. The boriding temperature and duration had significant effects of the phases formed within the boride layer. For a boriding temperature of 800 °C and durations of 2 and 4 h, Fe₂B was the only phase observed in the boride layer. In all other cases a double-phase boride layer consisting of FeB + Fe₂B was observed.
3. The hardness and thickness of the boride layers increased with increasing boriding temperature and time, while surface roughness decreased.
4. The corrosion resistance of the AISI H13 steel was improved 20–34 times depending on the boriding parameters. The greater thickness and decreased surface roughness of the boride layer that could be achieved at higher boriding temperatures and longer boriding durations generally resulted in better corrosion performance.
5. Potentiodynamic polarization curves revealed lower i_{corr} and E_{corr} values for the borided AISI H13 compared to untreated AISI 431. These results were consistent with open circuit potential measurements, indicating the possible potential of borided AISI H13 as an alternative to martensitic stainless steel.
6. The higher corrosion resistance of the borided AISI H13 over the untreated AISI H13 was attributed to B₂O₃ formation during corrosion.

References

1. ASM International, *ASM Handbook, Volume 1: Properties and Selection: Irons, Steels, and High-Performance Alloys* (Materials Park, ASM International, 1990), p. 1063. ISBN 978-0-87170-377-4
2. D.T. Llewellyn, R.C. Hudd, *Steels: Metallurgy and applications* (Elsevier, Amsterdam, 1998), p. 400. ISBN 978-0-7506-3757-2

3. B.S. Covino, S.D. Cramer, *Corrosion: Fundamentals, Testing and Protection*, vol. 13A, 10th edn. (ASM International, Materials Park, 2003), p. 1135
4. E. Bardal, *Corrosion and Protection* (Springer, New York, 2000), p. 315
5. J.R. Davis, *Surface Engineering for Corrosion and Wear Resistance* (CRC Press Taylor & Francis Group, Boca Raton, 2014), p. 289
6. A.G. Matuschka, *Boronizing* (Carl Hanser Verlag, München, 1980)
7. M.S. Gök, Y. Küçük, A. Erdoğan, M. Öge, E. Kanca, A. Günen, *Surf. Coat. Technol.* **328**, 54–62 (2017)
8. A. Günen, Y. Kanca, İ.H. Karahan, M.S. Karakaş, M.S. Gök, E. Kanca, A. Çürük, *Metall. Mater. Trans. A* **49**(11), 5833–5847 (2018)
9. J. Jibo, W. Yi, Z. Yi, Z. Qingdong, Z.Lei Qiongyu, *Surf. Coat. Technol.* **206**, 473–478 (2011)
10. G. Telasang, J. Dutta Majumdar, G. Padmanabham, I. Manna, *Surf. Coat. Technol.* **261**, 69–78 (2015)
11. G.K. Kariofillis, G.E. Kiourtsidis, D.N. Tsipas, *Surf. Coat. Technol.* **201**(1–2), 19–24 (2006)
12. A. Günen, E. Kanca, M. Demir, Y. Er, G. Sağlam, M.S. Gök, *Tribol. Trans.* **60**(2), 267–275 (2017)
13. C.M. Brakman, A.W.J. Gommers, E.J. Mittemeijer, *J. Mater. Res.* **4**(6), 1354–1370 (1989)
14. P. Asthana, H. Liang, M. Usta, A.H. Ucisik, *J. Tribol.* **129**(1), 1–10 (2007)
15. I. Campos, M. Palomar-Pardavé, A. Amador, C. VillaVelázquez, J. Hadad, *Appl. Surf. Sci.* **253**(23), 9061–9066 (2007)
16. A. Gunen, E. Kanca, *Matéria (Rio de Janeiro)* **22**(2), e11829 (2017)
17. M. Keddad, M. Ortiz-Dominguez, M. Elias-Espinosa, A. Arenas-Flores, J. Zuno-Silva, D. Zamarripa-Zepeda, O.A. Gomez-Vargas, *Metall. Mater. Trans. A* **49**(5), 1895–1907 (2018)
18. J. Zhong, W. Qin, X. Wang, E. Medvedovski, J.A. Szpunar, K. Guan, *Metall. Mater. Trans. A* (2018). <https://doi.org/10.1007/s11661-018-5002-8>
19. I. Gunes, M. Erdogan, A.G. Çelik, *Mater. Res.* **17**(3), 612–618 (2014)
20. I. Mejía-Caballero, J. Martinez-Trinidad, M. Palomar-Pardavé, M. Romero-Romo, H. Herrera-Hernández, O. Herrera-Soria, I.C. Silva, *J. Mater. Eng. Perform.* **23**(8), 2809–2818 (2014)
21. Y. Ergun, I. Gunes, M. Erdogan, N. Cankaya, *J. Nanosci. Nanotechnol.* **17**(12), 8946–8951 (2017)
22. M. Erdoğan, I. Gunes, A. Dalar, *Trans. Ind. Inst. Met.* **67**(2), 291–297 (2014)
23. H. Tavakoli, S.M. Khoie, *Mater. Chem. Phys.* **124**(2), 1134–1138 (2010)
24. P. Naemchanthara, P. Juijerm, *Metal. Mater. Trans. B* **49**(5), 2875–2880 (2018)
25. H. Wang, Y. Zhao, X. Yuan, K. Chen, R. Xu, *Phys. Procedia* **50**, 124–130 (2013)
26. R.L. Basso, H.O. Pastore, V. Schmidt, I.J. Baumvol, S.A. Abarca, F.S. de Souza, A. Spinelli, C.A. Figueroa, C. Giacomelli, *Corros. Sci.* **52**(9), 3133–3139 (2010)
27. Y. Liu, A. Li, X. Cheng, S.Q. Zhang, H.M. Wang, *Mater. Sci. Eng. A* **666**, 27–33 (2016)
28. A. Günen, E. Kanca, H. Çakir, M.S. Karakaş, M.S. Gök, Y. Küçük, M. Demir, *Surf. Coat. Technol.* **311**, 374–382 (2017)
29. Y. Iwabuchi, Y. Kobayashi, *Adv. Mater. Res.* **586**, 64–68 (2012)
30. A. Motallebzadeh, E. Dilektasli, M. Baydogan, E. Atar, H. Cimenoglu, *Wear* **328**, 110–114 (2015)
31. M. Erdogan, I. Gunes, *Matéria (Rio de Janeiro)* **20**(2), 523–529 (2015)
32. A.P. Krelling, J.C.G. Milan, C.E. da Costa, *Surf. Eng.* **31**(8), 581–587 (2019)
33. S. Şahin, *J. Mater. Process. Technol.* **209**(4), 1736–1741 (2009)
34. M.S. Karakaş, A. Günen, A.E. Kanca, E. Yilmaz, *Arch. Metall. Mater.* **63**(1), 159–165 (2018)
35. G. Bolelli, L. Lusvarghi, R. Giovanardi, *Surf. Coat. Technol.* **202**(19), 4793–4809 (2008)

Publisher's Note Springer Nature remains neutral with regard to jurisdictional claims in published maps and institutional affiliations.